Malaysian Journal of Chemistry, 2026, Vol. 28(1), 461-469
(Special Issue: *12th International Conference of the College of Science & 3rd Conference of Chemistry Department 2025*)

Comprehensive Study of TiO_2 Monolayer: A DFT Approach to Structural, Electronic, Optical, and Thermodynamic Characteristics

Worood S. Rasool and Mohammed A. Al-Kaabi*
Department of Physics, College of Science, Kerbala University, Karbala, Iraq
*Corresponding author (e-mail: mohammed.alkaabi@uokerbala.ed.iq)

Based on first-principles calculations, we have computed the optical and thermodynamic response of the monolayer using the CASTEP. During the structural optimization, it was confirmed that total energy was minimized (-39047.76 eV), and the values matched the reputable theoretical number quoted in the literature. We have investigated the structural stability of TiO_2, and the calculation confirms its stability due to the presence of positive frequencies in the spectrum. The thermodynamic behavior was examined generally as a function of temperature. However, few studies have systematically correlated the thermodynamic and optical responses of TiO_2 monolayers under identical DFT parameters. Our estimate of the Debye temperature was approximately 1300 K, indicating that lattice vibrations at room temperature are stiff, suggesting TiO_2 has reasonably good thermal conductivity behavior. The obtained band gap (2.93 eV) and Debye temperature were validated against previous DFT results, differing by less than 10 %. Interestingly, the TiO_2 reached the Dulong-Petit asymptote value at 600 K, which could compete with the well-known thermoelectric material, PbTe. Furthermore, the monolayer TiO_2 exhibits, confirming the model reliability. We have analyzed the dielectric properties and found that the TiO_2 absorbs light in the visible region, which is confirmed by the sharp peaks in optical spectra. Thus, the TiO_2 could serve as a potential candidate for optoelectronics and thermal applications.

Keywords: Thermodynamic properties, TiO_2 monolayer, DFT, phonon, band gap

Received: October 2025; Accepted: October 2025

A thriving field of research is the examination of the prospects of two-dimensional materials that have become popular with their wide variety of applications, which cover areas of energy storage, electronics, and many other fields. The popularity of the field is the result of the low-dimensional nature of those materials that are endowed with unprecedented properties [1, 2]. Nevertheless, fundamental concerns have been raised due to titania (TiO_2), which is considered a semiconductor with wide-gap properties. However, such properties can be recognized as the surface, which is catalytically active. Other prospects are long-standing and sustainable stability alongside the availability of the samples that are seen as single-crystal ones [3]. Among the wide range of semiconductors, TiO_2 becomes one of the most efficient and applicable photo-catalyst materials because of its properties of chemical stability, corrosion resistance, biocompatibility, non-toxicity, large surface area, cost effectiveness, and above all, the strong oxidizing power [4, 5].

Beyond photocatalysis, TiO_2-based 2D oxides are promising for Li-ion storage owing to their short diffusion paths and surface reactivity. This is due to the existence of the surface with its double properties of the paths that are short and active, and the sites that are the opposite, with their highly exposed activity [6, 7]. In recent years, high pressure has been concentrated as an extreme condition, given that numerous phases of TiO_2 have already been examined. Simultaneously, surface, quantum condiments, and size effects, as well as additional elements, are anticipated to generate unique characteristics in 2D nanostructured TiO_2 [6]. Many 2D TiO_2 phases have been computed, and there have been experimental attempts to reproduce these. The lepidocrocite (LNS) structure has been reported by a soft-chemical process [8]. The 2D structure has electron confinement in the Ti 3d orbitals and holes in the O 2p orbitals closer to the surface, which increases the photocatalytic activity by reducing the chance of charge carrier recombination. However, even with these advantages, 2D TiO_2 suffers from decreased performance because of its more significant band gap energy than its 3D predecessors [9, 10].

This study investigates the electronic properties, structural stability, optical characteristics, and thermodynamics of TiO_2 by electronic structure and phonon simulations, subsequently comparing the results with those of various TiO_2 phases.

†Paper presented at the 12th International Conference of the College of Science & 3rd Conference of Chemistry Dept. 2025

METHODOLOGY

In this study, we modeled the crystal structure of a TiO_2 ML using theoretically derived lattice parameters and incorporated relevant crystallographic data, including symmetry operations and space group information, from the CASTEP materials database. The TiO_2 ML is characterized by a trigonal crystal system and belongs to the space group P-3M1 (No. 164). The electronic configuration used in our simulations includes Ti: $3d^2 4s^2$ and O: $2s^2 2p^4$. In our first-principles calculations, a clear distinction was made between core and valence electrons, specifically, Ti core electrons ($1s^2 2s^2 2p^6$) and valence electrons ($3s^2 3p^6 3d^2 4s^2$), and O core ($1s^2$) and valence ($2s^2 2p^4$) electrons. All simulations were performed using the CASTEP code [11], a well-established first-principles computational tool based on plane-wave pseudopotential methods. CASTEP employs plane-wave basis sets for valence electrons and norm-conserving pseudopotentials to represent the interaction between valence electrons and ionic cores. in this work, we employed the generalized gradient approximation (GGA) framework with the exchange-correlation of Perdew–Burke-Ernzerhof (PBE) functional for better calculations and results [12]. Using a plane-wave (PW) basis set with a convergence test of a kinetic energy cutoff of 750 eV. Self-consistent field (SCF) iterations were performed until the total energy convergence threshold reached 1×10^{-6}, and the maximum force on atoms was reduced below 0.03 eV/Å. To eliminate interactions between periodic images along the out-of-plane direction, a vacuum spacing of 15 Å was introduced perpendicular to the ML. Brillouin zone integrations were carried out using a Γ-centered Monkhorst–Pack grid of 6×6×1 for geometry optimization and a 12 × 12 × 1 mesh to calculate both density of states (DOS) and optical properties calculations [13]. Using the Broyden–Fletcher–Goldfarb–Shanno (BFGS) algorithm for optimization of minimum energy and lattice parameters, this method was fully optimized, ensuring a minimum-energy configuration for subsequent analysis [14, 15].

Optical properties are intrinsically linked to a material's electronic, thermal, and magnetic characteristics. Different optical parameters were computed and provide complete insight into a material's interaction with light energy [16, 17]. The complex dielectric function is represented by equation (1) and plays a central role in defining these properties [18].

$$\varepsilon(\omega) = \varepsilon_1(\omega) + i\varepsilon_2(\omega) \quad (1)$$

At the atomic level, polarization effects arise from the displacement of electron clouds under an external field. In extended solids, the cumulative polarization from all atoms defines the macroscopic dielectric response [19, 20]. These interactions, especially the absorption of photons, can be understood through time-dependent perturbation theory, where the excitation of electrons from occupied to unoccupied states is driven by the photon energy. Optical absorption occurs when an incident photon has sufficient energy to promote an electron from an occupied state to an unoccupied one. When a large number of photons are capable of facilitating such transitions, this results in a pronounced peak in the imaginary component of the dielectric function, indicating strong absorption at that photon energy [18].

Using Density Functional Perturbation Theory (DFPT), the phonon spectrum over the full Brillouin zone can be obtained by analyzing how the total energy changes in response to small atomic displacements [21, 22]. With the complete phonon spectrum, one can derive the phonon dispersion and density of states. These, in turn, enable the calculation of various thermodynamic properties within the quasi-harmonic approximation, including Helmholtz free energy, enthalpy, entropy, and heat capacity [23-27].

RESULTS AND DISCUSSION

Structure and Stability of TiO_2

The optimized TiO_2 ML structure calculations were performed for a 4×4 supercell shown in Figure 1 below. The calculated lattice constant (a_0) for TiO_2 ML is 2.98 Å. We found a good agreement with the already available literature on TiO_2 (2.99 Å) [28] Å. The Ti-O bond lengths varied from 1.96 to 2.57Å(see Table 1). These are consistent with previously reported experimental and theoretical values [29, 30]. The minimum energy is equal to (-39047.76 eV) compared with the theoretical study [31].

The structural stability of the TiO_2 ML was further evaluated by examining its dynamical stability through phonon spectrum analysis. Since two-dimensional materials often experience instability caused by unbalanced forces when disturbed, this can manifest as imaginary frequencies in their phonon spectra, indicating potential reconstructive or martensitic phase transformations [32]. Figure 2 presents the calculated phonon band structure for the TiO_2 ML. The acoustic phonon modes near the Γ point exhibit typical behavior observed in 2D materials [33], where the longitudinal and transverse acoustic modes show linear dependence on the wave vector (k), and the out-of-plane acoustic mode follows a quadratic (k^2) dependence. Based on this analysis, the TiO_2 ML is considered dynamically stable. No negative frequencies were detected throughout the Brillouin zone, confirming dynamic stability within ±0.1 THz accuracy.

Thermodynamic Properties

Thermodynamic properties such as heat capacity, enthalpy, free energy, Debye temperature (θ_D), and entropy were calculated for the TiO_2 ML as functions of temperature using equations of state. When the temperature is below the θD, quantum mechanical effects significantly influence the heat capacity and related thermodynamic properties. For the TiO_2 ML, θD increases rapidly as the temperature rises from 0 to 1000 K, eventually leveling off near 1300 K, as illustrated in Figure 3(a). The Debye temperature was extracted from the phonon density of states using the Debye-Einstein model, which should be explicitly included here. This relatively high θD may contribute to the material's high thermal conductivity, reported to be approximately 609.5 $mW \cdot m^{-1} \cdot K^{-1}$ [34]. The computed θ^D (≈1300 K) exceeds that of bulk anatase (≈950 K), suggesting enhanced lattice stiffness in the monolayer. Additionally, the elevated θ_D indicates that phonons predominantly govern the specific heat below this temperature. Figure 3(b) depicts how the heat capacity at constant volume (CV) varies with temperature for the TiO_2 ML. At low temperatures, CV exhibits a significant change and follows a T^3 dependence. Once the θ_D is reached, the heat capacity stabilizes and remains nearly constant regardless of further temperature increases. The θ_D increases and then stabilizes at approximately 1000 K. Below this saturation temperature, the heat capacity reaches about 260 J mol^{-1} K^{-1}, remaining nearly constant as the temperature rises above 1000 K. In addition to the θD and CV, other thermodynamic properties such as enthalpy, free energy, and entropy were calculated based on phonon dispersion data for the TiO_2 ML Figure 3(c). As temperature increases, the enthalpy of the system rises due to the greater kinetic and potential energy contributions, while the free energy of the TiO_2 ML decreases with temperature. This behavior is consistent with thermodynamic principles, where increasing temperature leads to higher internal energy but lower free energy.

Atomic Charges

In DFT studies, partial atomic charges are commonly calculated as part of the comprehensive analysis of TiO_2 ML properties. Although neither first-principles methods nor experiments can directly and precisely determine partial atomic charges [35], the distribution of charge density within a molecule plays a crucial role in determining its physical and chemical behavior. Various experimental and theoretical techniques allow for detailed examination of electron distributions. To relate this information to specific atomic sites, the concept of atoms carrying partial charges within a molecule has been developed. This approach helps explain properties that depend on the distribution of electron density. Among the methods used, (i) the partial equalization of orbital electronegativity (PEOE) technique estimates atomic charges by equalizing the electronegativities of atomic orbitals [36]. On the other hand, (ii) Mulliken population analysis assigns electron density to atoms based on their contributions to molecular orbitals [37] {see Figure (4)}. In this work, Mulliken charges were calculated, yielding values of −0.67 e for oxygen and 1.35 e for titanium, which are compared to Hirshfeld charges of −0.29 e for oxygen and 0.58 e for titanium in the TiO_2 ML.

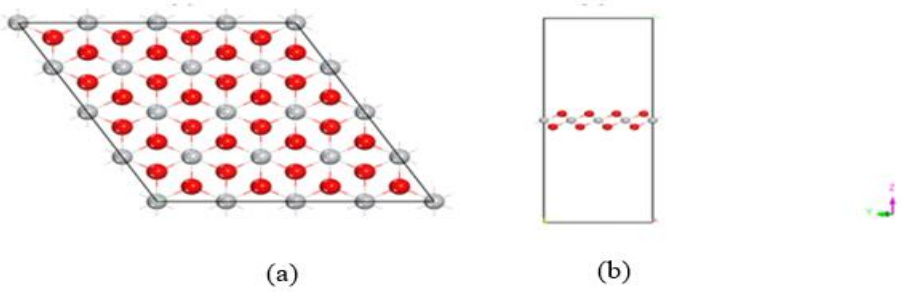

Figure 1. The optimized TiO_2 ML (a)top view(b)side view.

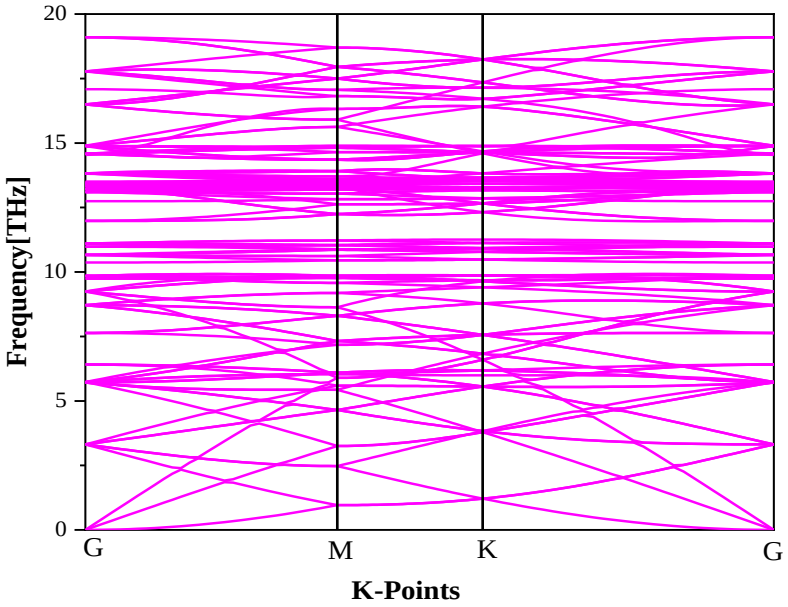

Figure 2. Phonon band structure of TiO_2 ML obtained using DFPT.

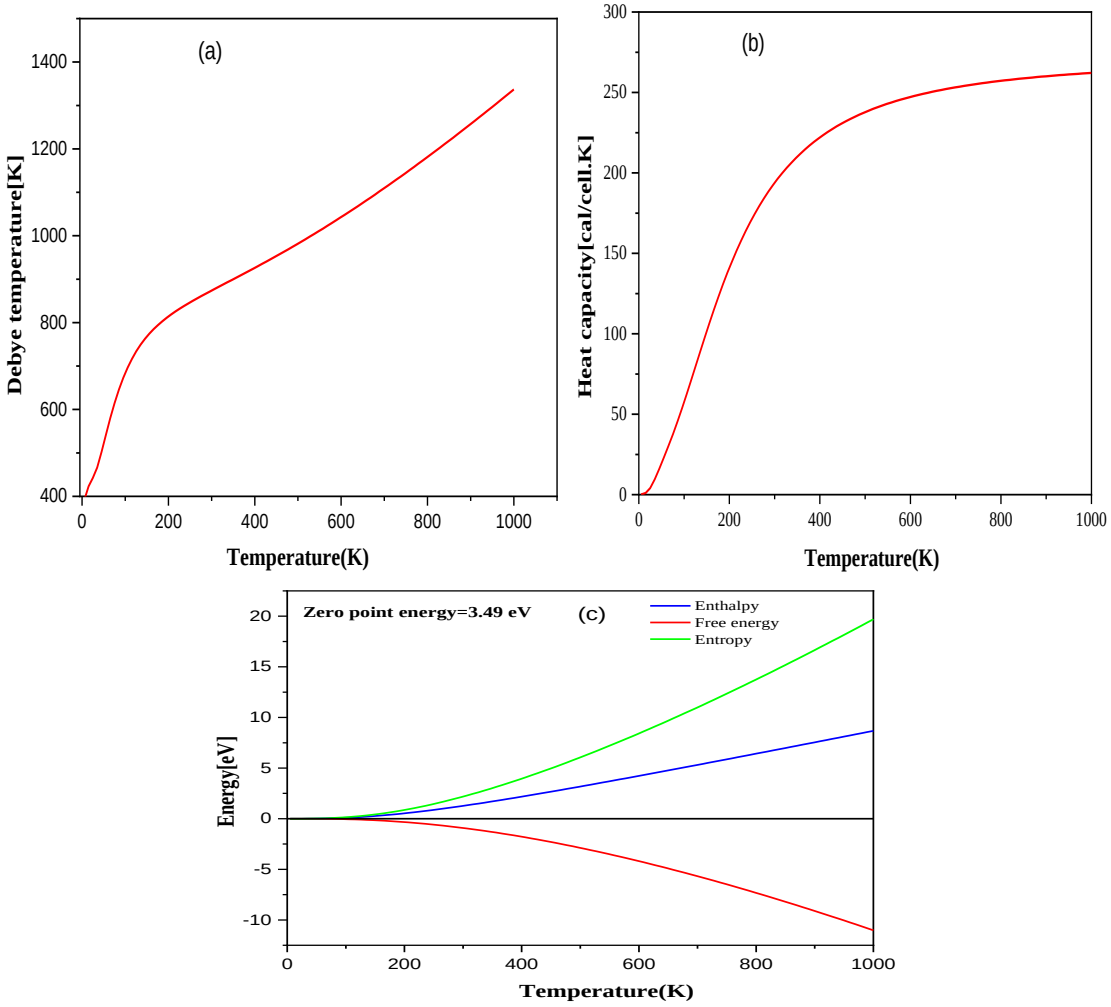

Figure 3. The calculated (a) Debye temperature, (b)heat capacity, and (c) the variation of enthalpy, entropy, and free energy with temperature for TiO_2 ML.

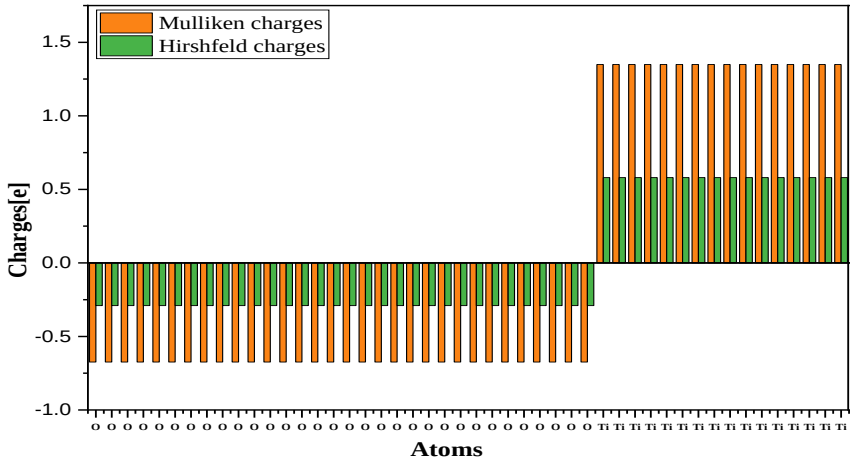

Figure 4. The charge density for TiO_2 ML.

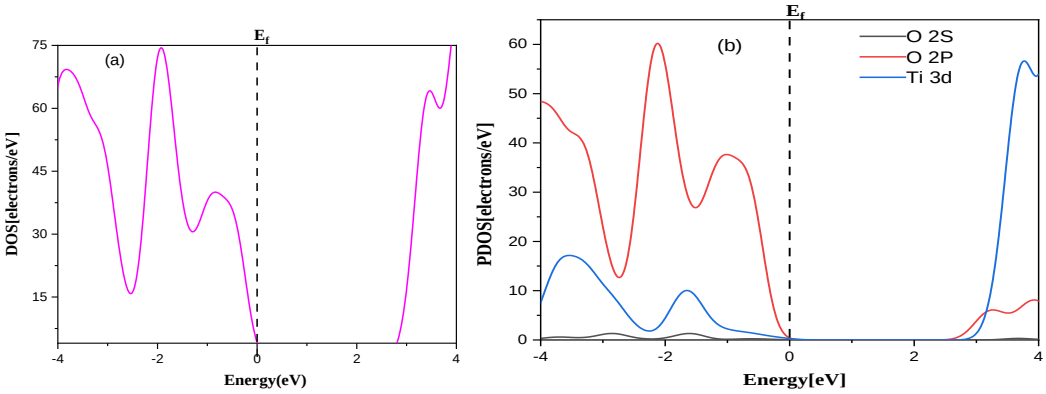

Figure 5. The calculated (a) Density of states (DOS), (b) Partial density of states (PDOS) for TiO_2 ML.

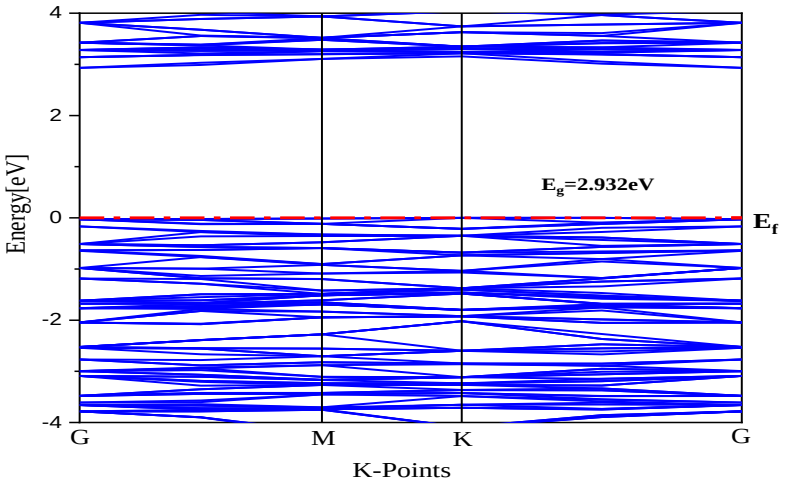

Figure 6. Band structure of TiO_2 ML.

Electronic Structure

Understanding such variations is essential, as they reflect the sensitivity of the electronic properties to computational parameters and structural configurations. Significant computational effort was directed toward characterizing the electronic structure of the TiO_2 ML. The calculated density of states (DOS) and projected density of states (PDOS) provide detailed insight into the distribution of electronic states and the contributions of specific atomic orbitals. These results are particularly useful for evaluating the photocatalytic potential of the material, as they reveal bandgap modifications and highlight the orbital character of the valence and conduction bands.

The combined effects influence both the charge carrier recombination rate and the absorption edge, which are key factors directly related to the photoactivity of the material [38]. As shown in Figure 5, and in agreement with other theoretical studies, DFT calculations indicate that the conduction band minimum (CBM) and valence band maximum (VBM) are mainly composed of Ti 3d and O 2p orbitals, respectively. These findings were further supported by the identification of O 2p states near the VBM and Ti 3d states near the CBM in the TiO_2 ML. The Fermi level (E_f) was set as the reference at 0 eV. The dominance of O-2p states near the VBM implies hole localization on oxygen sites, beneficial for oxidative photocatalysis.

The calculated band gap for TiO_2 was found to be 2.932 eV (see Figure 6), which is slightly larger than the reported value of 2.65 eV [28]. This discrepancy can be attributed to factors such as the self-interaction error in electron correlation, limitations related to the derivative discontinuity in DFT, and the hybridization effects arising from excitonic quantum confinement in nanoscale structures compared to bulk materials [39].

Optical Properties

The signatures seen in the imaginary part of the dielectric function mainly arise from optical transitions among the 2p orbitals of oxygen atoms in the valence band and the d orbitals of titanium atoms in the conduction band. In contrast, the real portion has a static dielectric constant of approximately 2.5, as shown in Figure 7(a). The static $\varepsilon_1(0)$ is lower than bulk anatase (~3.5), consistent with dielectric suppression in 2D systems.

Electromagnetic wave propagation yields positive values of the real portion, while negative values mark regions in which the material does not support wave propagation but rather absorption. The peak maximum of the real portion occurs within the visible portion of the electromagnetic spectrum and quickly diminishes toward higher energies until it becomes negative, and absorption begins to dominate. The primary absorption peak at ≈ 3 eV corresponds to $\lambda \approx 410$ nm (visible region). The associated imaginary part corresponds to photon absorption and is representative of the electronic structure of the crystal. Sharp peak transitions occurring in the imaginary part represent transitions of charge carriers from occupied states to unoccupied states; this intensity is evident even over the region between 1 eV and 10 eV.

Therefore, the TiO_2 ML has excellent potential for optoelectronic applications in both the visible and ultraviolet regions. The refractive index is an important optical property that characterizes the propagation of light in a medium, where the real part of the refractive index indicates the phase speed of electromagnetic (EM) waves in the material, while the imaginary part, sometimes referred to as the extinction coefficient, characterizes the amount of intensity loss of waves as they propagate through the material. As demonstrated in Figure 7(b), the reflectivity operates in the same manner as the real part of the dielectric function, from which reflectivity is calculated. The calculated static reflectivity for the TiO_2 ML shows a sharp peak at approximately 0.12 (near-infrared), followed by a gradually decreasing reflectance as energy increases into the visible and ultraviolet regions. The optical conductivity $\sigma(\omega)$ measures how well a material can conduct current in the presence of optical excitation and is derived from the complex dielectric function. As shown in Figure 7(c), the optical conductivity increases linearly with photon energy until approximately 7 eV, with decreasing conductivity thereafter, some oscillatory behavior, and flattening beyond that energy range. Beyond the decline of $\sigma(\omega)$ reflects interbond transition saturation and diminished carrier mobility.

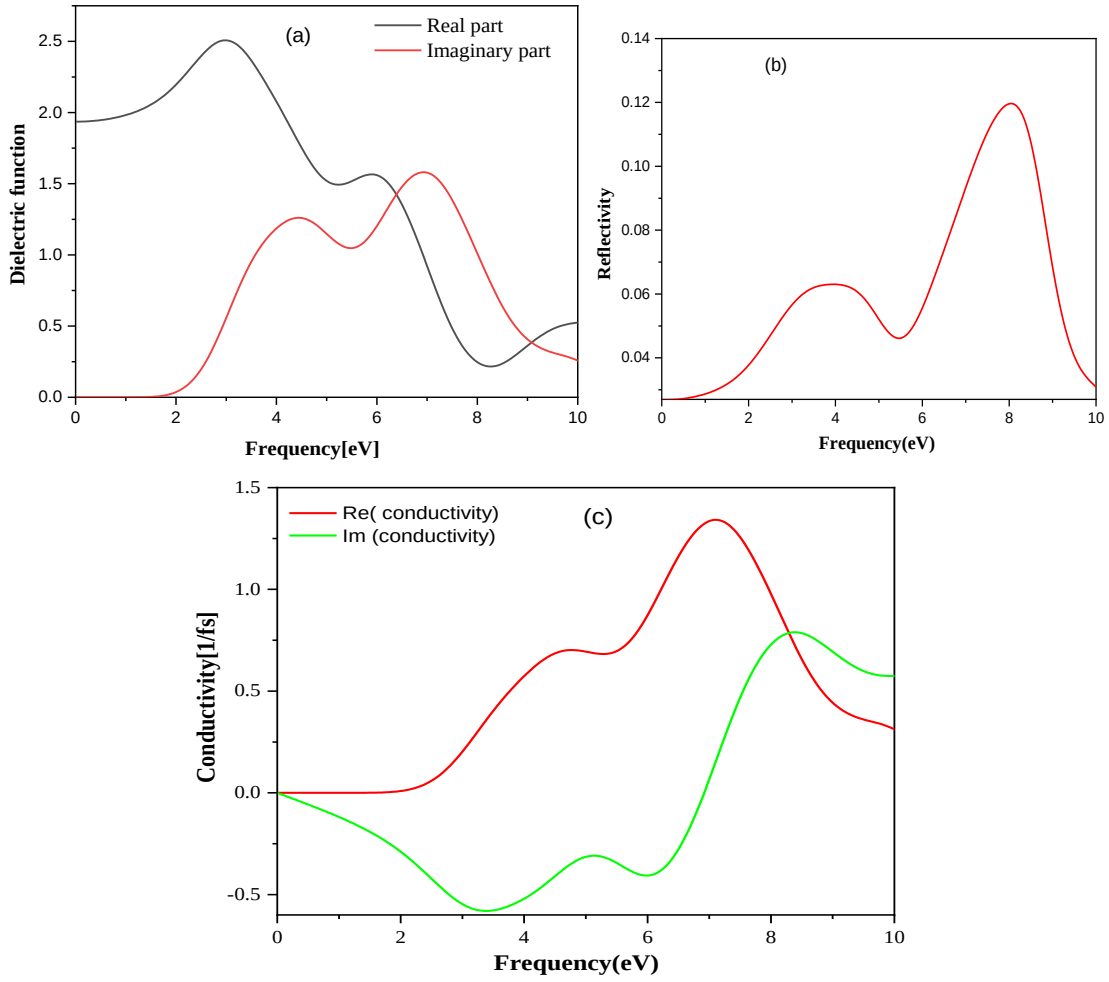

Figure 7. The calculated (a) Dielectric function, (b) Reflectivity, and (c) Conductivity for TiO_2 ML.

Table1. Lattice constant, bond length, and bond angle for TiO_2 ML.

Structure	Lattice constant[A^0]	Bond length[A^0]		Bond angle[deg]
		Ti-O	Ti-O- Ti	O - Ti - O
TiO_2	2.98	1.96	98.04	98.01

CONCLUSION

In this study, we employed DFT to investigate the structural, electronic, optical, and thermodynamic properties of a TiO_2 ML. The key findings are as follows: (i) The optimized structural parameters are consistent with previously reported theoretical and experimental data, reflecting the expected values based on the inherent symmetry of the system. (ii) The electronic band structure reveals a direct bandgap of approximately 2.932 eV, as obtained using the GGA-PBE exchange-correlation functional, confirming the semiconducting nature of the TiO_2 ML. (iii) The complex dielectric contribution from the p and d states. The complex dielectric function of TiO_2 ML is anisotropic concerning light polarization, with its real and imaginary parts exhibiting more pronounced variation with energy crystalline directions. The same occurs for the optical absorption. (iv) The thermodynamic properties of TiO_2 ML are presented by its enthalpy, entropy, free energy, and heat capacity. These insights highlight TiO_2 ML as a potential candidate for nanoscale thermoelectric and optoelectronic devices, motivating further

investigation under strain or doped conditions. Future work should explore defect engineering and transition-metal doping to tailor band alignment and phonon scattering for optimized performance.

REFERENCES

1. Wang, S. L., Luo, X., Zhou, X., Zhu, Y., Chi, X., Chen, W. (2017) Fabrication and properties of a free-standing two-dimensional titania. *Journal of the American Chemical Society*, **139(43)**, 15414–15419.

2. Szczęśniak, D., Gnyp, J. T. and Kielak, M. (2025) Semiconducting and superconducting properties of 2D hexagonal materials. *Preprint ArXiv:2502.14567*.

3. Mete, E., Uner, D., Gülseren, O. and Ellialtıoğlu, Ş. (2009) Pt-incorporated anatase TiO_2 (001) surface for solar cell applications: First-principles density functional theory calculations. *Physical Review B-Condensed Matter and Materials Physics*, **79(12)**, 125418.

4. Yan, H., Wang, X., Yao, M. and Yao, X. (2013) Band structure design of semiconductors for enhanced photocatalytic activity: The case of TiO_2. *Progress in Natural Science: Materials International*, **23(4)**, 402–407.

5. Bokare, A. and Erogbogbo, F. (2021) Photocatalysis and Li-Ion Battery Applications of {001} Faceted Anatase TiO_2-Based Composites, **4(3)**, 500–530.

6. Liu, B., Gu, B., Wang, J., Li, A., Zhang, M. and Shen, Z. (2022) Tuning the defects of two-dimensional layered carbon/TiO_2 superlattice composite for fast lithium-ion storage. *Materials*, **15(5)**, 1625.

7. Szczęśniak, R. (2025) The Superconducting State of the LiC6 Compound: The Effective Triangular Lattice Model. *Acta Physica Polonica A ISSN 1898-794X*, **147(3)**, 236–236.

8. Wang, L., Wei, D., Kang, S., Xie, X., Shi, Y. and Liu, S. (2018) Two-dimensional Titania: Structures and properties predicted by first principle calculation. *The Journal of Physical Chemistry C*, **122(40)**, 22911–22919.

9. Asikainen, K., Alatalo, M., Huttula, M. and Sasikala Devi, A. A. (2023) Tuning the Electronic Properties of Two-Dimensional Lepidocrocite Titanium Dioxide-Based Heterojunctions. *ACS Omega*, **8(47)**, 45056–45064.

10. Asikainen, K., Alatalo, M., Huttula, M. and Aravindh, S. A. (2025) Tailoring the electronic properties of TiO_2 monolayers for solar-driven catalysis through transition metal doping. *Catalysis Today*, **447**, 115144.

11. Segall, M., Lindan, P. J., Probert, M. A., Pickard, C. J., Hasnip, P. J., Clark, S. (2002) First-principles simulation: ideas, illustrations and the CASTEP code. *Journal of Physics: Condensed Matter*, **14(11)**, 2717.

12. Perdew, J. P., Burke, K. and Ernzerhof, M. (1996) *Physical Review Letters*, **77(18)**, 3865.

13. Monkhorst, H. J. and Pack, J. D. (1976) Special points for Brillouin-zone integrations. *Physical Review B*, **13(12)**, 5188.

14. Yuan, Y. -X. (1991) A modified BFGS algorithm for unconstrained optimization, IMA. *Journal of Numerical Analysis*, **11(3)**, 325–332.

15. Najgebauer, M., Chwastek, K. and Koprivica, B. (2025) Application of Scaling Algorithms in the Analysis of Energy Losses Under Non-sinusoidal Excitations. *Acta Physica Polonica A ISSN 1898-794X*, **147(3)**, 200–200.

16. Mahmood, T., Malik, H., Batool, R., Perveen, Z., Saleemi, F. and Rasheed, H. (2017) Elastic, electronic and optical properties of anatase TiO_2 under pressure: A DFT approach. *Chinese Journal of Physics*, **55(4)**, 1252–1263.

17. Aydin, A. and Dede, B. (2025) Structural, Electronic, Thermodynamic and Nonlinear Optical Properties of a Novel Ce (III) Complex with Ferrocenyl Dithiophosphonate. *Acta Physica Polonica A*, **148(1)**, 3–3.

18. Abed, Y. and Mostaghni, F. (2016) Simulation Investigations of Structural, Electronic, Optical and Elastic Properties of the CuxTi1-xO_2. *Nanoscience and Nanotechnology*, **6(4)**, 62–67.

19. Giustino, F. (2014) Materials modelling using density functional theory: properties and predictions. *Oxford University Press*.

20. Meftah, A. and Cheridi, N. (2025) Structural Modifications in Vitreous SiO_2 Induced by N and Ar Ion Irradiation: Competing Roles of Nuclear and Electronic Energy Losses. *Acta Physica Polonica A*, **148 (1)**, 34–34.

21. Baroni, S., De Gironcoli, S., Dal Corso, A. and Giannozzi, P. (2001) Phonons and related crystal properties from density-functional perturbation theory. *Reviews of Modern Physics*, **73 (2)**, 515.

22. Garus, S., Sochacki, W., Leśniak, D. and Garus, J. (2025) The Dynamic Stability of Quasi-Periodic and Aperiodic Multi-Segment Columns.

Acta Physica Polonica A ISSN 1898-794X, **147 (3)**, 176–176.

23. Colmenero, F., Fernández, A. M., Cobos, J. and Timón, V. (2018) Thermodynamic properties of uranyl-containing materials based on density functional theory. *The Journal of Physical Chemistry C*, **122(10)**, 5254–5267.

24. Berski, S., Jarosik, M. and Gruszka, K. (2025) Electron-Phonon Interaction and Superconductivity in NaSn 3 Intermetallic Compound. *Acta Physica Polonica A ISSN 1898-794X*, **147 (3)**, 253–253.

25. Lakel, S., Elhamra, F., Almi, K. and Meradji, H. (2015) Density functional perturbation theory calculations of vibrational and thermodynamic properties of Zn1-xBexO alloys. *Materials Science in Semiconductor Processing*, **40**, 209–217.

26. Bolen, E., Deligoz, E. and Ozisik, H. (2021) Origin of low thermal conductivity in monolayer PbI2. *Solid State Communications*, **327**, 114223.

27. Eddekkar, M., El-Ouaddi, H., Labrag, A., Bghour, M., Soussi, A., Zakaria, J. (2024) DFT-based (HSE06) investigation of band gap engineering: Optoelectronic, mechanical and thermodynamic insights in Cs2AgBiY6 (YBr, I) for photovoltaic applications. *Micro and Nanostructures*, **190**, 207840.

28. Rasmussen, F. A. and Thygesen, K. S. (2015) Computational 2D materials database: electronic structure of transition-metal dichalcogenides and oxides. *The Journal of Physical Chemistry C,* **119(23)**, 13169–13183.

29. Sato, H., Ono, K., Sasaki, T. and Yamagishi, A. (2003) First-principles study of two-dimensional titanium dioxides. *The Journal of Physical Chemistry B*, **107(36)**, 9824–9828.

30. Horn, M., Schwebdtfeger, C. and Meagher, E. (1972) Refinement of the structure of anatase at several temperatures. *Zeitschrift für Kristallographie-Crystalline Materials*, **136 (1-6)**, 273–281.

31. Lamiel-Garcia, O., Ko, K. C., Lee, J. Y., Bromley, S. T. and Illas, F. (2017) When anatase nanoparticles become bulklike: properties of realistic TiO_2 nanoparticles in the 1–6 nm size range from all electron relativistic density functional theory based calculations. *Journal of Chemical Theory and Computation*, **13(4)**, 1785–1793.

32. Paul, J., Singh, A., Dong, Z., Zhuang, H., Revard, B., Rijal, B. (2017) Computational methods for 2D materials: discovery, property characterization, and application design. *Journal of Physics: Condensed Matter*, **29(47)**, 473001.

33. Zhang, X., Qiao, X. -F., Shi, W., Wu, J. -B., Jiang, D. -S. and Tan, P. -H. (2015) Phonon and Raman scattering of two-dimensional transition metal dichalcogenides from monolayer, multilayer to bulk material. *Chemical Society Reviews*, **44(9)**, 2757–2785.

34. Batmunkh, M., Tanshen, M. R., Nine, M. J., Myekhlai, M., Choi, H., Chung, H. (2014) Thermal conductivity of TiO_2 nanoparticles based aqueous nanofluids with an addition of a modified silver particle. *Industrial & Engineering Chemistry Research*, **53(20)**, 8445–8451.

35. Bachrach, S. M. (1994) Population analysis and electron densities from quantum mechanics. *Reviews in Computational Chemistry*, 171-228.

36. Gasteiger, J. and Marsili, M. (1980) Iterative partial equalization of orbital electronegativity—a rapid access to atomic charges. *Tetrahedron*, **36(22)**, 3219–3228.

37. Mulliken, R. S. (1955) Electronic population analysis on LCAO–MO molecular wave functions. I, *The Journal of Chemical Physics*, **23(10)**, 1833–1840.

38. Zhukovskii, Y. F., Piskunov, S., Lisovski, O., Bocharov, D. and Evarestov, R. (2017) Doped 1D Nanostructures of Transition-metal Oxides: First-principles Evaluation of Photocatalytic Suitability. *Israel Journal of Chemistry*, **57(6)**, 461–476.

39. Mori-Sánchez, P., Cohen, A. J. and Yang, W. (2008), Localization and Delocalization Errors in Density Functional Theory format and Implications for Band-Gap Prediction. *Physical Review Letters*, **100(14)**, 146401.